Article ID: 1003－6326(2005)04－0828－06

High-pressure sintering and magnetic properties of $Fe_{86}Zr_{11-x}Nb_xB_3$ (x= 5.5, 6) amorphous alloys①

LU Bin(卢 斌)[1], YI Dan-qing(易丹青)[1],
YAN Biao(严 彪)[2], YIN Jun-lin(殷俊林)[2], LIU Yan(刘 岩)[3],
LIU Hui-qun(刘会群)[1], WU Wei(吴 炜)[1], MA Rui(马 瑞)[1]
(1. School of Materials Science and Engineering, Central South University, Changsha 410083, China;
2. Institute of Materials Science and Engineering, Tongji University, Shanghai 200092, China;
3. Shanghai Institute of Ceramics, Chinese Academy of Sciences, Shanghai 200050, China)

Abstract: The thermal stability of milling $Fe_{86}Zr_{11-x}Nb_xB_3$ (x= 5.5, 6) melt-spun strip powders and the influence of high-pressure sintering conditions on phase component and grain size of bulk alloys were investigated by X-ray diffractometry(XRD), differential scanning calorimetry(DSC) and scanning electron microscopy(SEM). The results show that milling melt-spun powder remains in the amorphous state, and the crystallization temperature of which is 480－530 ℃, the apparent activation energy E_p of crystallization process is 294.1－219.5 kJ/mol. The increasing Nb content can increase crystallization temperature and decrease E_p. Under the sintering conditions of 5.5 GPa/3 min, when P_w is 1 150 W, single phase α-Fe nanocrystalline (20.6－26.7 nm) bulk alloy with relative density higher than 99.0% can be obtained. Under the sintering conditions of 5.5 GPa/1 150 W/3 min, the magnetic properties of these nanocrystalline bulk alloys are $Fe_{86}Zr_{5.5}Nb_{5.5}B_3$ alloy, B_s= 1.15 T, H_c= 5.08 kA·m^{-1}; $Fe_{86}Zr_5Nb_6B_3$ alloy, B_s= 1.26 T, H_c= 4.27 kA·m^{-1}.

Key words: Fe-based alloy; amorphous alloy; thermal stability; high-pressure sintering; bulk alloy; nanocrystalline; magnetic properties

CLC number: TG 139.8; TF 123.3 **Document code:** A

1 INTRODUCTION

Fe-based nanocrystalline soft magnetic alloys become the focus in the world because of their excellent soft magnetic properties and high saturation induction. In engineering applications, soft magnetic alloys are usually used in bulk form with complex shape. However, nanocrystalline soft magnetic alloys in engineering applications are prepared through the crystallization of amorphous alloy which is controlled by melt spinning, accordingly the shape and size of the alloys are restricted in a high degree. In order to enlarge the application range of this kind nanocrystalline alloy, it is necessary to prepare amorphous or nanocrystalline bulk alloys from these amorphous powder or thin ribbons. It was reported that amorphous or nanocrystalline soft magnetic bulk alloys were prepared by high-pressure solidification method[1-4], thermal extrusion method[5-7], explosion molding method[8, 9] and spark plasma sintering method (SPS)[10-12]. In these powder metallurgy methods, high sintering pressure can promote nucleation rate of crystallization and restrain grain growth significantly, so as to obtain nanocrystalline alloys[13], therefore high-pressure solidification method becomes a suitable method to prepare nanocrystalline bulk alloys. However special high-pressure equipment and bulk shape size become the constrained factors of development of this technique and its applications. At present, hexahedral crown fluid high-pressure equipment provides a technical basis for studying and preparing large size nanocrystalline soft magnetic bulk alloys because quite great progresses have been acquired at high pressure of synthesis cavity and large size.

In this paper, under the research basis of thermal stability of $Fe_{86}Zr_{11-x}Nb_xB_3$ (x= 5.5, 6) amorphous alloys, the influence of high-pressure sintering conditions on phase component and grain size and magnetic properties were analyzed, which provided a theoretical basis for its engineering applications.

2 EXPERIMENTAL

Vacuum induction furnace was used to melt

① **Foundation item:** Project(0452NM086) supported by the Tackling Key Science and Technology Program of Shanghai, China
Received date: 2004－10－08; **Accepted date:** 2005－01－24
Correspondence: LU Bin, Associate Professor, PhD; Tel: +86-731-8836319; E-mail: luoffice@mail.csu.edu.cn

ingots of alloys with nominal composition $Fe_{86}Zr_{11-x}Nb_xB_3$ (x= 5.5, 6), and amorphous ribbons were prepared by single roller melt spinning in argon atmosphere. Amorphous ribbons were pulverized into 50 - 150 μm powder by QM - 1SP high energy milling machine. Graphite heating die (d20 mm × 10 mm) filled with 10 g powder assembled in phrophyllite cubic bulk composed the high pressure cavity, the sketch of which is shown in Fig. 1. High pressure sintering experiment was performed on HTDS - 032A hexahedral crown fluid pressure machine, and the sintering pressure (p) was 5.5 GPa, heating power P_w was 530 - 1 150 W, heating time was 3 min, holding time was 3 min. Phase component was analyzed by Dmax-rA X-ray diffractometer, and Scherrer equation ($D = 0.91\lambda/(B\cos\theta)$) was used to evaluate average grain size value D of bulk alloys. Morphology of powder was observed by JSM - 5600LV scanning electron microscope (SEM). The thermal stability analysis of samples was performed on STA449C differential scanning calorimeter (DSC), and the heating-up rate was 5 - 20 ℃/min. The microstructure of samples was analyzed by H - 800 transmission electron microscope (TEM). Archimedes' method was used to measure the density of samples. Measure of magnetic properties was performed on LDJ9600 vibrating sample magnetometer (VSM) with maximum magnetizing field H_{max}= 1.0 × 103 kA · m^{-1}.

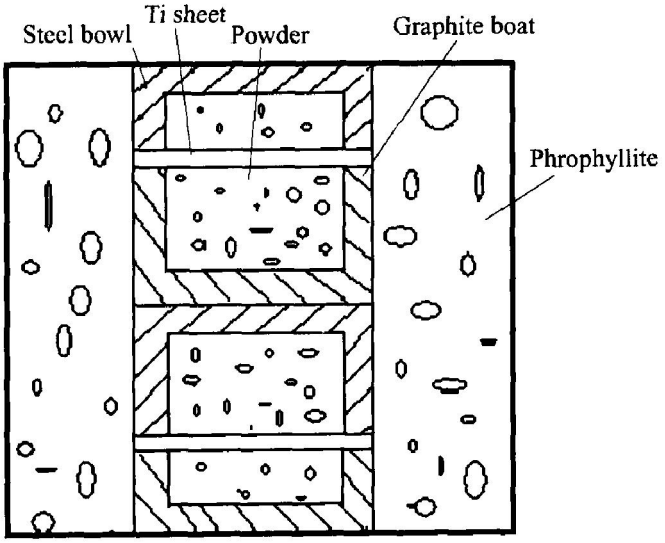

Fig. 1 Sketch of structure of high pressure cavity

3 RESULTS AND ANALYSIS

3.1 Milling melt-spun powder

SEM observation shows that after milling $Fe_{86}Zr_{11-x}Nb_xB_3$ (x = 5.5, 6) melt-spun amorphous ribbons the morphology of powder is near lamella, and XRD analysis shows that these milling powders still remain in the amorphous state (see Fig. 2(a)).

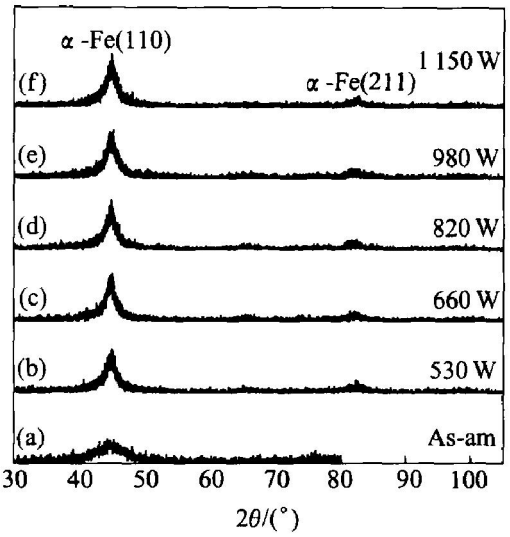

Fig. 2 XRD patterns of melting-spun powder and sintering samples under different P_w (p= 5.5 GPa, t= 3 min)

Fig. 3 shows the DSC curves of $Fe_{86}Zr_{11-x}Nb_xB_3$ (x= 5.5, 6) amorphous powder. It can be seen that two exothermal peaks appear in every DSC curve, in which, the first peak temperature value of $Fe_{86}Zr_{5.5}Nb_{5.5}B_3$ alloy is 480 - 510 ℃, the other peak temperature value is 760 - 793 ℃; the first peak temperature value of $Fe_{86}Zr_5Nb_6B_3$ alloy is 500 - 530 ℃, the other is 770 - 800 ℃. In addition, two peak temperature values of two alloys increase with the increasing heating-up rate, however, the first peak temperature value of $Fe_{86}Zr_{5.5}Nb_{5.5}B_3$ alloy is lower than that of $Fe_{86}Zr_5Nb_6B_3$ alloy, the second peak temperature value of two alloys is the same. It is known that the first exothermal peak is induced by the precipitation of αFe phase from amorphous matrix, the second one is due to the decomposition of residual amorphous phase at high temperature[6]. According to the relationship between heating-up rate and peak temperature[14], apparent reaction activation energy of amorphous crystallization is evaluated as follows:

$$\frac{d\ln(\Phi/T_p^2)}{d(1/T_p)} = -\frac{E_p}{R} \quad (1)$$

where Φ is heating-up rate (K/min), T_p is peak temperature (K), E_p is reaction activation energy (J/mol), R is mole gas constant (8.314 J/mol · K). Relationship between $\ln(\Phi/T_p^2)$ and $(1/T_p)$ of two alloys is shown in Fig. 4. It can be seen that $\ln(\Phi/T_p^2)$ and $(1/T_p)$ have good linear relationship, the apparent reaction activation energy of alloys calculated by slope rate are: for $Fe_{86}Zr_{5.5}Nb_{5.5}B_3$ alloy E_p= 294.1 kJ/mol, for $Fe_{86}Zr_5Nb_6B_3$ alloy E_p = 219.5 kJ/mol.

From the analyses mentioned above, for $Fe_{86}Zr_{11-x}Nb_xB_3$ (x = 5.5, 6) amorphous alloys, with the increasing x(Nb) content, the crystalliza-

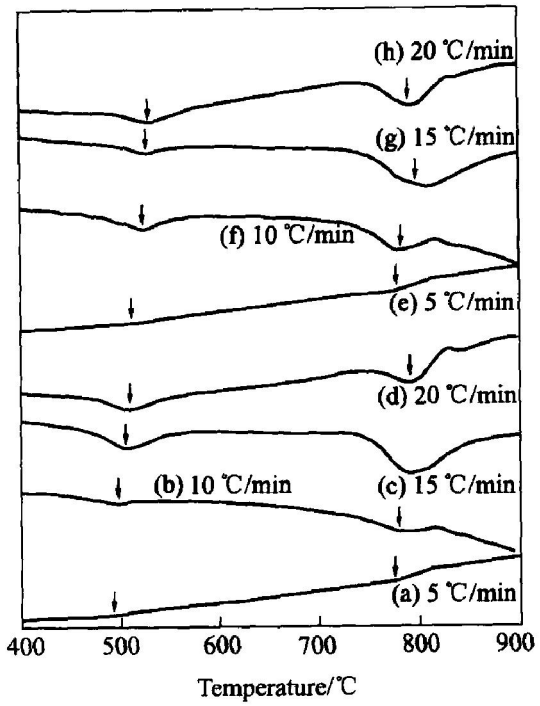

Fig. 3 DSC curves of amorphous powders under different heating-up rates
(a), (b), (c), (d) —Sample $Fe_{86}Zr_{5.5}Nb_{5.5}B_3$;
(e), (f), (g), (h) —Sample $Fe_{86}Zr_5Nb_6B_3$

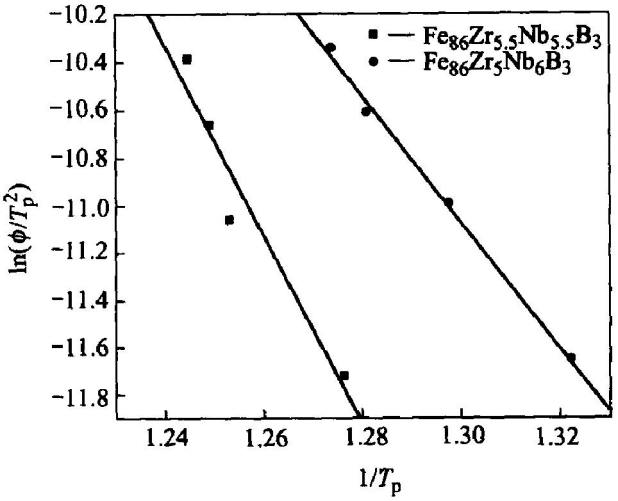

Fig. 4 Relationship between $\ln(\varphi/T_p^2)$ and $(1/T_p)$ of amorphous powder

tion temperature of alloys increase and the crystallization reaction activation energy decrease significantly, however it doesn't affect the phase decomposition of residual amorphous phase at high temperature. Thermal stability analysis shows that in order to obtain αFe phase nanocrystalline alloy, it is feasible that high-pressure sintering temperature is selected at 500 – 770 ℃.

3.2 Preparation of bulk alloys

During high-pressure sintering process, considering the relationship between heating temperature and heating power P_w, the range of P_w was 530 – 1 150 W. Under the sintering conditions of 5.5 GPa/3 min, the influence of P_w on relative density of $Fe_{86}Zr_{11-x}Nb_xB_3$ (x = 5.5, 6) sintering samples is shown in Fig. 5, from which it can be seen that with increasing P_w, when $P_w \leqslant 820$ W, the relative density of samples increases significantly and then increases slowly; when P_w = 1 150 W, the relative density of samples reaches 99%. Compared with that, the relative density of $Fe_{86}Zr_5Nb_6B_3$ alloy increases quickly. All the samples have high densification, which is related to the decreasing viscosity and increasing plasticity happened during amorphous crystallization[6].

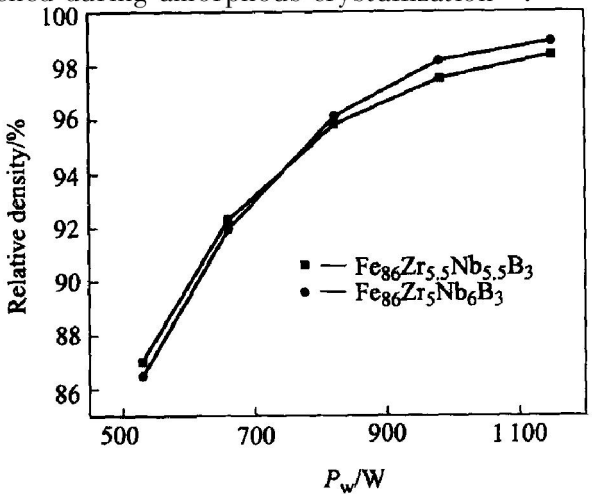

Fig. 5 Influence of P_w on relative density of sintering samples
(p = 5.5 GPa, t = 3 min)

Figs. 2(b) – (f) show the XRD patterns of $Fe_{86}Zr_{5.5}Nb_{5.5}B_3$ sintering samples under different P_w, the regularity of XRD patterns of $Fe_{86}Zr_5Nb_6B_3$ sintering samples is similar to that of $Fe_{86}Zr_{5.5}Nb_{5.5}B_3$ sintering samples. From XRD patterns it can be seen that, these samples are composed of single αFe phase, every diffraction peak shows the broadening characteristic. According to Scherrer equation, average grain size D values of αFe phase in $Fe_{86}Zr_{11-x}Nb_xB_3$ (x = 5.5, 6) alloys are evaluated, and the results are given in Fig. 6. With the increasing P_w, D values of all samples have the similar increasing tendency, while D values of $Fe_{86}Zr_5Nb_6B_3$ sintering samples are larger than those of $Fe_{86}Zr_{5.5}Nb_{5.5}B_3$ sintered samples. All the D values are 10.2 – 15.4 nm.

Fig. 7 shows the typical TEM images and SAD patterns of $Fe_{86}Zr_{11-x}Nb_xB_3$ (x = 5.5, 6) sintering samples under the sintering conditions of 5.5 GPa/1 150 W/3 min. From Figs. 7(a) and (b) it can be known that in $Fe_{86}Zr_{5.5}Nb_{5.5}B_3$ bulk alloy nanocrystalline grains with homogeneous size precipitate in matrix, D value of which is 20.6 nm. Diffusing diffraction ring appearing in the SAD patterns of this alloy shows that the matrix still remains in

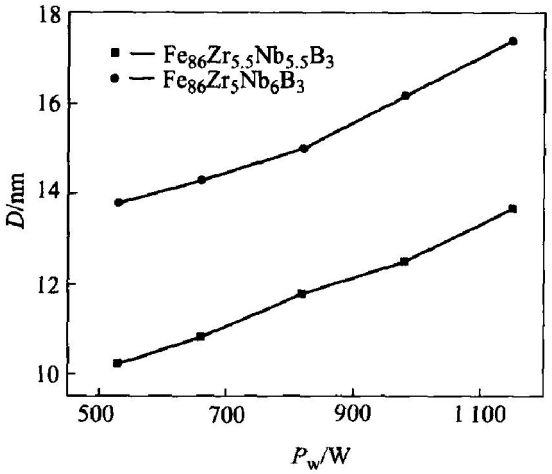

Fig. 6 Effect of P_w on grain size of αFe phase of $Fe_{86}Zr_{11-x}Nb_xB_3$ (x= 5.5, 6) alloys

the amorphous state. The analysis shows that the diffraction rings from inner to exterior correspond to {110}, {200} and {211} plane diffraction of αFe solid solution phase precipitated from matrix. From Figs. 7(c) and (d), it can be seen that microstructure of $Fe_{86}Zr_5Nb_6B_3$ alloy is similar to that of $Fe_{86}Zr_{5.5}Nb_{5.5}B_3$ alloy, the difference is that D value 26.7 nm of the former alloy is larger than that of the latter. It is observed that αFe nanocrystalline grains precipitating from amorphous matrix appear as elliptic morphology, which would affect the coercive force of bulk alloys. Comparing the results of Scherrer equation calculating with TEM images, it can be seen that calculation results of grains size are larger than that of quantified metallographic measured results of TEM images, the error range is 33 – 34%. From the description mentioned above it can be seen that, high sintering pressure can evidently promote the nucleation rate of amorphous crystallization process as well as restrain the growth of grains and is facilitated to obtain densified nanocrystalline bulk alloy, so hexahedral crown high-pressure technique is a simple method with high efficiency and low cost to prepare nanocrystalline bulk alloy.

3.3 Magnetic property of bulk alloys

Fig. 8 shows the hysteresis loops of $Fe_{86}Zr_{11-x}Nb_xB_3$ (x= 5.5, 6) sintering samples under the

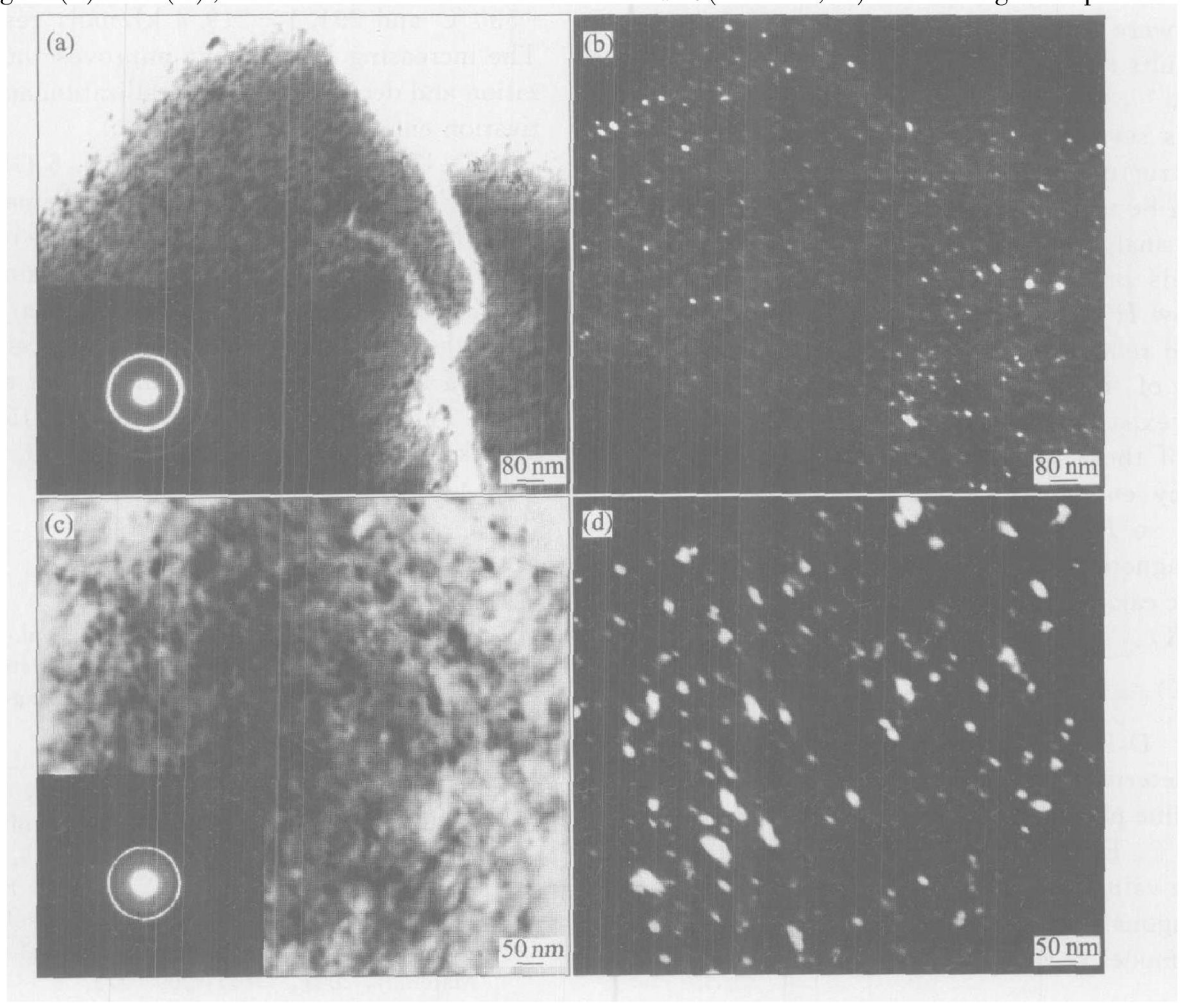

Fig. 7 TEM images and SAD patterns of sintering samples
(a), (b) —Bright field image and dark field image of $Fe_{86}Zr_{5.5}Nb_{5.5}B_3$;
(c), (d) —Bright field image and dark field image of $Fe_{86}Zr_5Nb_6B_3$
(p= 5.5 GPa, P_w= 1 150 W, t= 3 min)

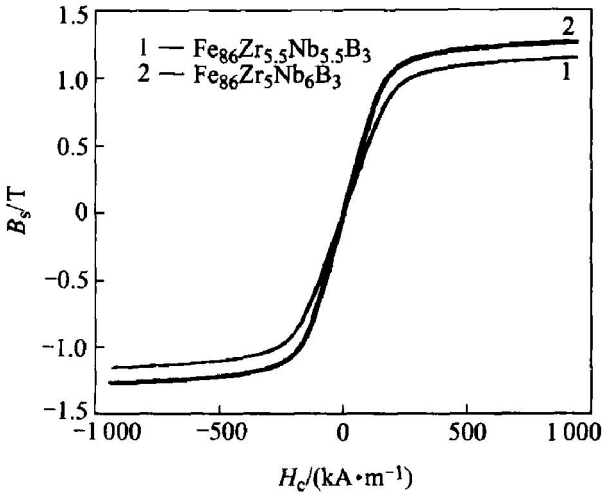

Fig. 8 Hysteresis loop of sintering samples (p= 5.5 GPa, P_w= 1 150 W, t= 3 min)

sintering conditions of 5.5 GPa/1 150 W/3 min. From the curves saturation induction B_s and coercive force H_c were calculated as follows, $Fe_{86}Zr_{5.5}Nb_{5.5}B_3$ alloy: B_s= 1.15 T, H_c= 5.08 kA · m^{-1}; $Fe_{86}Zr_5Nb_6B_3$ alloy: B_s= 1.26 T, H_c= 4.27 kA · m^{-1}. After Nb content was increased from 5.5% to 6.0%, the magnetic properties of sintering bulk alloys were improved evidently. Compared with the results reported by Kawamura et al[2] and Kojima et al[6], the H_c of as-received bulk alloys in this paper is several orders of magnitude higher. The microstructure of bulk alloys is composed of single phase αFe nanocrystalline. According to the theoretical analysis of nanocrystalline soft magnetic materials proposed by Herzer[15], these samples have low H_c. Herzer[15] considered that, in an exchanged relating characteristic length L_{ex}^0 large amount of nanocrystalline soft magnetic grains should exist, and the magnetocrystalline anisotropy K of these grains can be averaged into a low value by enough exchange couple between these grains, so H_c of materials is decreased and good soft magnetic properties can be obtained. Simple statistic calculation shows that the average value of K is $\langle K \rangle$:

$$\langle K \rangle \approx K\left[\frac{D}{L_{ex}^0}\right]^6 = \frac{K^4 \cdot D^6}{A^3} \quad (2)$$

where D is grain size; exchange related length L_{ex}^0 is determined by exchange stiffness A of nanocrystalline phases and anisotropy content K, $L_{ex}^0 = (A/K)^{1/2}$. Eqn. (2) shows that, when $D < L_{ex}^0$, the average value of anisotropy content is proportional to hexagonal equation of grain size D. If spinning rotary model is valid, H_c can be described as follows:

$$H_c = \frac{P_c \cdot \langle K \rangle}{J_s} \approx P_\mu \cdot \left[\frac{K^4 \cdot D^6}{J_s \cdot A^3}\right] \quad (3)$$

where P_c and P_μ are proportional constant, and J_s is saturation magnetization.

Evidently, the decrease of grain size to a certain degree leads to small average or effective anisotropy of materials, so, H_c of materials is decreased. Microstructure sensitive property H_c is not only related to grain size, but also related to morphology of grains, crystal defect, and second phases. High H_c results in large moving resistance of magnetic domain wall. The existence of holes and reverse domain boundaries caused by incomplete densification of samples during sintering process induces hindrance of magnetic domain wall, therefore coercive force increases, and internal microstrain is introduced during high-pressure sintering process and oxidation of powders also affect H_c of sintering bulk alloy. In addition, αFe phase nanocrystalline grains with evident directivity and elliptic shape are disadvantage to decrease H_c. So, several reasons lead to the increase of H_c.

4 CONCLUSIONS

1) After milling powders are pulverized, $Fe_{86}Zr_{11-x}Nb_xB_3$ (x= 5.5, 6) melt-spun powders still remain in the amorphous state, their crystallization temperature and apparent activation energy are 480 – 530 ℃ and 294.1 – 219.4 kJ/mol, respectively. The increasing Nb content improves the crystallization and decreases the crystallization apparent activation energy.

2) Under the conditions of 5.5 GPa/3 min, when P_w= 1 150 W, single phase αFe nanocrystalline (20.6 – 26.7 nm) bulk alloys with relative density higher than 99.0% can be obtained.

3) Under the conditions of 5.5 GPa/1 150 W/3 min, the magnetic properties of as-received single phase αFe nanocrystalline bulk alloys are as follows: $Fe_{86}Zr_{5.5}Nb_{5.5}B_3$ alloy, B_s= 1.15 T, H_c= 5.08 kA · m^{-1}; $Fe_{86}Zr_5Nb_6B_3$ alloy, B_s= 1.26 T, H_c= 4.27 kA · m^{-1}.

REFERENCES

[1] Kawamura Y, Takagi M, Senoo M, et al. Preparation of bulk amorphous alloys by high temperature sintering under a high pressure[J]. Mater Sci Eng, 1988, 98: 415 – 418.

[2] Kawamura Y, Inoue A, Kojima A, et al. Consolidation of amorphous Fe-Zr-B powders by hot-pressing method[J]. Journal of the Japan Society of Powder and Powder Metallurgy, 1995, 42(1): 40 – 46.

[3] LU Bin, YI Dan-qing, LIU Yan, et al. Formation of $Fe_{73.5}Cu_1Nb_3Si_{13.5}B_9$ nanocrystalline soft magnetic bulk alloys in high pressure[J]. Journal of Inorganic Materials, 2004, 19(4): 269 – 273.

[4] LU Bin, YI Dan-qing, LIU Yan, et al. Preparation of $Fe_{84}Nb_7B_9$ nanocrystalline soft magnetic bulk alloy under high-pressure[J]. The Chinese Journal of Nonferrous Metals, 2004, 14(2): 173 – 178. (in Chinese)

[5] Kawamura Y, Takagi M, Akai M. A newly developed

warm extrusion technique for compacting amorphous alloy powders[J]. Mater Sci Eng, 1988, 98: 449 - 452.

[6] Kojima A, Horikiri H, Kawamura Y, et al. Production of nanocrystalline b. c. c. Fe-Nb-B bulk alloys by warm extrusion and their magnetic properties[J]. Mater Sci Eng, 1994, A179 - A180: 511 - 515.

[7] Kojima A, Horikiri H, Makino A, et al. Soft-magnetic porerties of nanocrystalline bcc Fe-(Nb, Zr)-B bulk alloys consolidated by warm extrusion[J]. Mater Trans JIM, 1995, 36(7): 945 - 951.

[8] Sato T, Taniguchi T, Kondo K, et al. Effect of shock duration time on magnetic properties of dynamically compacted amorphous powder[J]. Journal of the Japan Society of Powder and Powder Metallurgy, 1988, 35 (3): 96 - 100.

[9] QIU Jun, XIE Zi-zhang, YANG Rang, et al. The magnetic properties of the explsive consolidating amorphous powder[J]. Journal of University of Science and Technology Beijing, 1994, 16(4): 330 - 334.

[10] Kojima A, Mizushima T, Makino A, et al. Soft magnetic properties of bulk nanocrystalline $Fe_{90}Zr_7B_3$ alloys consolidated by spark-plasma sintering[J]. Journal of the Japan Society of Powder and Powder Metallurgy, 1996, 43(5): 613 - 618.

[11] Shen B L, Kimura H, Inoue A A, et al. Consolidation of Fe-Co-Ga-P-C-B glassy powders by spark-plasma-sintering and their magnetic properties[J]. Journal of the Japan Society of Powder and Powder Metallurgy, 2001, 48(9): 858 - 862.

[12] LU Bin, YI Dan-qing, LIU Yan, et al. SPS sintering and magnetic properties of $Fe_{70}Cr_8Mo_2Si_5B_{15}$ amorphous[J]. Journal of Functional Materials, 2004, 35: 698 - 699.

[13] LIU Xiao-min, YAO Bin, SU Wen-hui. A thermodynamic study on the crystallization processes of amorphous $(Fe_{0.99}Mo_{0.01})_{78}Si_9B_{13}$ alloy under high pressure[J]. Chinese Journal of High Pressure Physics, 1997, 11(4): 260 - 265.

[14] LU Chang-wei, XI Tong-geng. Thermal Analysis Mass Spectrography[M]. Shanghai: Shanghai Scientific and Technical Literature Press, 2002. 104 - 105.

[15] Herzer G. Nanocrystalline soft magnetic materials [J]. J Magn Magn Mater, 1992, 112: 258 - 262.

(Edited by LI Xiang-qun)